Title: Electrode-Skin Impedance Imbalance Measured in the Frequency Domain

Authors: Benjamin C. Fortune [a], Christopher G. Pretty [a], Chris J. Cameron [a], Lachlan R. McKenzie [a], Logan T. Chatfield [a], and Michael P. Hayes [b]

Affiliations:
[a] Centre for Bioengineering, University of Canterbury, Christchurch, New Zealand
[b] Department of Electrical and Computer Engineering, University of Canterbury, Christchurch, New Zealand

Corresponding author: Benjamin Fortune, e-mail: ben.fortune@pg.canterbury.ac.nz

---

Abstract

Objective
To measure the magnitude and phase imbalance of the electrode-skin interface for silver/silver chloride (Ag/AgCl) and silver (Ag) electrode pairs, highlighting the need to balance both the magnitude and phase of the electrode-skin interface.

Methods
The electrode-skin impedance imbalance between two electrodes placed on ten healthy subjects was recorded over a frequency range of 1 Hz–100 kHz, using three electrode configurations: Ag/AgCl electrodes without skin preparation ($Ag/AgCl_{NSP}$), Ag/AgCl electrodes with skin preparation ($Ag/AgCl_{SP}$), and Ag electrodes with skin preparation ($Ag_{\text{-}SP}$). A compensation network was developed to simulate impedance imbalance reduction using the experimental data.

Results
The mean electrode-skin impedance imbalance at 50 Hz was $(37.6 \pm 47.1)\,k\Omega$ and (15.0 ± 18.3) degrees using the $Ag/AgCl_{NSP}$ electrode configuration; $(4.52 \pm 7.65)\,k\Omega$ and (4.6 ± 6.9) degrees using the $Ag/AgCl_{SP}$ electrode configuration; and $(36.2 \pm 45.1)\,k\Omega$ and (3.4 ± 3.6) degrees using the $Ag_{\text{-}SP}$ electrode configuration. The compensation network resulted in a mean reduction in impedance imbalance over the bioelectrical signal range (1 Hz–500 Hz) of 284.3 kΩ and 11.9 degrees; 4.6 kΩ and 6.2 degrees; 86.7 kΩ and 2.5 degrees for the $Ag/AgCl_{NSP}$, $Ag/AgCl_{SP}$ and $Ag_{\text{-}SP}$ electrode configurations respectively.

Conclusion
This study confirmed that the electrode-skin impedance imbalance can be large, and varies between subjects. Although abrasive skin preparation reduces the electrode-skin impedance imbalance, it does not guarantee a balanced electrode-skin interface, therefore, balancing the electrode-skin impedance using a compensation network has the potential to decrease bioelectrical signal interference.

Significance
As bioelectrical signal interference is a function of electrode-skin impedance imbalance, to improve noise immunity of bioelectrical signal recordings, added compensatory impedance is required to balance the electrode-skin interface.

Keywords: Electrode-skin interface, Electrode-tissue interface, impedance, compensation, balancing, crosstalk, sEMG, EMG

1 Introduction

Bioelectrical instrumentation is used to measure weak bioelectrical signals. However, these signals can be contaminated by several forms of interference: mains supply (common-mode) interference, mains supply (differential-mode) interference due to common-mode conversion, and bioelectrical crosstalk from signals generated by sources in close proximity. Therefore, bioelectrical instrumentation requires a high common-mode rejection ratio (CMRR) to suppress common-mode noise [1]. This requires well matched circuitry. However, well matched circuitry is difficult to achieve due to imbalances between the individual electrode-skin interfaces [2,3]. An impedance mismatch will result in common-mode interference being converted into a differential-mode signal due to the potential divider effect [2–4]. Although the imbalance of the electrode-skin impedance impacts many bioelectrical recording techniques (e.g. electromyography (EMG), electroencephalography (EEG) and electrocardiography (ECG)), this paper focuses on surface electromyography (sEMG).

Displacement and conduction currents flow through the electrode leads due to being capacitively coupled to the AC mains power supply [2,3,5]. Since the recording device has a high input impedance, the displacement and conduction currents will flow through the electrode-skin interface and to ground through a reference electrode. The resulting differential-mode voltage is proportional to the imbalance of the electrode-skin impedance, and becomes superimposed with the bioelectrical signal.

Crosstalk in sEMG is the phenomenon of one muscle's signal influencing the recording of another [6–8], making it difficult to measure a contraction from a single muscle. Intramuscular electrodes are also affected by crosstalk [9]. A common method of reducing crosstalk is the tripolar electrode configuration [10–13]. However, the efficacy of this method is limited by electrode-skin impedance imbalance [10] and the proximity of the influencing muscle [14].

Bioelectrical interference and crosstalk is a function of the electrode-skin impedance imbalance. If the electrode-skin impedance can be measured, compensatory impedance may be used to reduce the effect of interference. As the electrode-skin interface is time dependent [15], this method would be applied in real-time during the recording process, minimising the variability associated with each individual subject and recording session.

This paper focuses on measuring the magnitude and phase imbalance of the electrode-skin interface, confirming the need for compensatory impedance balancing for improved bioelectrical signal quality. This paper is divided as follows: Section 2 provides background knowledge on the electrode-skin interface; Section 3 describes the method undertaken to obtain, process and verify the data; Section 4 outlines the results of this study; Section 5 discusses the results of this study; and Section 6 provides a conclusion.

2 Background

Bioelectrical recording typically requires at least two recording electrodes and a reference electrode, producing multiple electrode-skin interfaces. The electrode-skin interface is an electrochemical transducer that exhibits nonlinear frequency, temporal and current-density characteristics with a hysteresis response [16], all that are dominated by the large variable impedance of the skin itself [17]. Moreover, an impedance imbalance of the electrode-skin interface can be caused by both physiological changes in the subject and imperfections related to the electrodes.

These characteristics are often unpredictable [17,18] and must be understood before attempting to measure the impedance of the electrode-skin interface.

The physiological variability related to the subject can be due to the sweat glands and ducts, the epidermis layer of skin [5] or local changes in temperature at the electrode site [19]. The variability of the electrode can be due to the fabrication process, resulting in electrodes with different surface properties and non-homogeneous electrode gel [19]. The electrode-skin impedance has an inverse temporal and frequency relationship, except for heavily abraded skin, which exhibits an increase in impedance with time. Therefore, repeated, simultaneous measurements of the electrode-skin interfaces is the most reliable and effective method to understand the impedance behaviour at the interface [18]. Between applying the electrodes to a subject, and recording bioelectrical signals, the impedance of each electrode-skin interface changes and can continue to change with time, with controversy about whether this alters the electrode-skin impedance imbalance [4,18], or not [17]. High impedance related to poor skin condition can be lessened using skin preparation [15,20]: ranging from cleaning the skin with alcohol to abrading the skin surface with sand paper. However, the effect on the imbalance of the electrode-skin impedance due to skin preparation is unknown.

While there are large limitations of bioelectrical sensing caused by the imbalance of the electrode-skin impedance, only a few researchers have focused on measuring the impedance imbalance of the interface. Electrode-skin impedance imbalances of 50% of the individual electrode-skin interface is common, typically resulting in an imbalance of 10 kΩ at 50 Hz [18], producing an unacceptable level of interference of 200 μV peak-to-peak [3]. However, imbalances as high as 58 kΩ can be present [17].

Other researchers have focused on measuring the impedance of the electrode-skin interface, but the work was not not intended for measuring the impedance imbalance between multiple electrodes, with limitations including: assuming a balanced electrode-skin interface [21–23]; limited frequency span [15,21,22]; measuring the individual electrode-skin impedance, without reporting the impedance imbalance between electrodes [15,24]; or performing an impedance balancing method on an electrode-electrode interface in a saline solution, reducing the variability associated with the human body [19].

Usually researchers measure the electrode-skin interface using excitation frequency sweeps, typically in the range of 1 Hz–1 kHz [17,18,22], one study used higher excitation frequencies, up to 50 kHz [24], but the impedance imbalance in this case was not measured. When the individual electrode-skin impedance is measured, it is common to only report the magnitude, where only one study reported the phase [15]. To the authors' knowledge, there are no studies that measure the electrode-skin impedance imbalance of human subjects with the intent of adding compensatory impedance to balance the interface. Therefore, this paper presents a study measuring both the magnitude and phase of the electrode-skin impedance imbalance for multiple subjects, skin preparation levels and a wide frequency range.

3 Methods

To measure the electrode-skin impedance imbalance, the voltage across the individual electrode-skin interface and the series current must be measured during a frequency sweep, where each excitation frequency (f_k) excites the interface for a period T. Applying a discrete-time Fourier transform (DTFT) to the voltage and current signals for each frequency, k, results in a complex

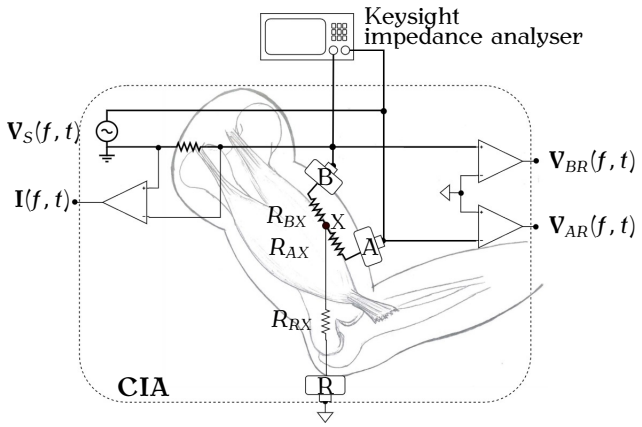

Figure 1: High level schematic of how the custom impedance analyser (CIA) can measure the individual impedance of the electrode-skin interface.

voltage across each electrode-skin interface and the series current. These complex values form the frequency dependent impedance of the individual electrode-skin interface.

3.1 Data Collection and Impedance Extraction

Measuring the individual electrode-skin impedance was achieved using a custom impedance analyser (CIA), with a stimulation path through electrodes A and B, measuring both electrodes separately with respect to the reference electrode, Figure 1: where $V_S(f,t)$ is the excitation voltage of the CIA as a function of excitation frequency and time; $I(f,t)$ is the series current of the CIA as a function of excitation frequency and time; $V_{AR}(f,t)$ is the voltage measured across one electrode-skin interface (electrode A) with respect to the reference electrode (electrode R) as a function of excitation frequency and time; $V_{BR}(f,t)$ is the voltage measured across the second electrode-skin interface (electrode B) with respect to the reference electrode as a function of excitation frequency and time; R_{AX}, R_{BX} and R_{RX} are the resistances associated with the dermis and subcutaneous layers of the skin between the respective electrodes; X is a common node connection for the resistances associated with the dermis and subcutaneous layers of the skin. As the reference electrode is connected to a high input impedance, no current flows through R_{RX} and the reference electrode contact impedance, Z_{R_C}, therefore, $V_{AR}(f,t)$ and $V_{BR}(f,t)$ are referenced to the subcutaneous node X. The individual electrode-skin impedances (Z_A, Z_B) are the sum of the electrode contact impedances (Z_{A_C}, Z_{B_C}) and the resistance associated with the dermis and subcutaneous layers,

$$Z_A(f) = Z_{A_C}(f) + R_{AX} = \frac{V_{AR}(f)}{I(f)}\,, \tag{1}$$

$$Z_B(f) = Z_{B_C}(f) + R_{BX} = \frac{V_{BR}(f)}{I(f)}\,. \tag{2}$$

The CIA was developed using Analog Device's AD9838 Direct Digital Synthesis device that produces the sinusoidal excitation voltage $V_S(f,t)$, with controllable amplitude and frequency.

The amplitude of $V_S(f,t)$ was varied in the range of 50–800 mV peak-to-peak. The CIA produced 40 logarithmically spaced discrete frequencies, where $V_S(f,t)$, $I(f,t)$, $V_{AR}(f,t)$ and $V_{BR}(f,t)$ were sampled at 125 kS/s to 3.125 MS/s, with an excitation period of 10 s for frequencies below 10 Hz and 1 s for the remaining frequencies using a Saleae Logic Analyser, Logic Pro 16. For each known excitation frequency, a DTFT was applied to $I(f,t)$, $V_{AR}(f,t)$ and $V_{BR}(f,t)$,

$$\widehat{V}_{AR}(f) = \sum_{n=0}^{N-1} V_{AR}(f_k, t) \times \mathrm{e}^{-j2\pi f_k n \Delta t}, \tag{3}$$

where N is the length of $V_{AR}(f_k, t)$ and Δt is the sampling period. This process was performed in MATLAB (R2019b, MathWorks) for each of the 40 frequencies, resulting in a complex array for the two electrode voltages and the series current. The impedance associated with the individual electrode-skin interfaces can then be determined,

$$\mathbf{Z}_A(f) = \frac{\widehat{V}_{AR}(f)}{\widehat{I}(f)}, \tag{4}$$

$$\mathbf{Z}_B(f) = \frac{\widehat{V}_{BR}(f)}{\widehat{I}(f)}. \tag{5}$$

3.2 Data Validation

3.2.1 Passive Circuitry

To validate the efficacy of the impedance measurement method, passive circuitry was used as a proxy device under test (DUT), Figure 2. The proxy DUT was designed to model a pair of single or double exponential electrode-skin interfaces. However, the single exponential interfaces were used in this study. The proxy DUT was formed from known component values (measured using a Tonghui TH2822E handheld LCR meter). This permitted comparison of the theoretical impedance to the data captured using the CIA. The theoretical impedance is given by $Z_{T_A}(f) = R_1 + R_2 \| Z_{C_1}$ and $Z_{T_B}(f) = R_4 + R_3 \| Z_{C_2}$, where $Z_{T_A}(f)$ and $Z_{T_B}(f)$ are the theoretical impedances of the first and second electrodes respectively.

Three data sets were obtained using the CIA and the proxy DUT, with component values outlined in Table 1. This process highlighted that the CIA was affected by parasitic inductance, as the CIA could not accurately measure the phase at frequencies above 10 kHz and the magnitude above 100 kHz. To quantify the accuracy of the system, a root mean square error (RMSE) was applied to the data captured using the CIA, $Z_{\mathrm{CIA}}(f)$, and the theoretical impedance, $Z_T(f)$,

$$\mathrm{RMSE} = \frac{1}{K} \sqrt{\sum_{k=0}^{K-1} \left\{ Z_{\mathrm{CIA}}(f_k) - Z_{\mathrm{T}}(f_k) \right\}^2}, \tag{6}$$

where K = 40 (the number of discrete excitation frequencies). The RMSE was scaled by the mean of the theoretical impedance to produce a normalised root mean square error (NRMSE),

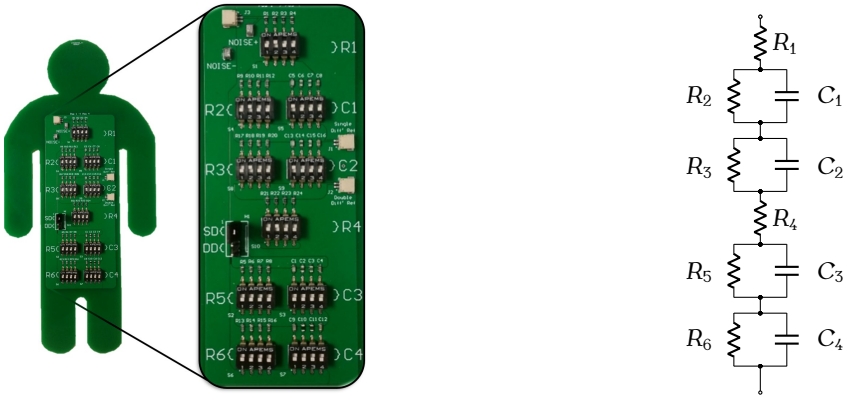

(a) (b)

Figure 2: (a) Passive circuitry used to emulate the human electrode-skin interface using a single or double exponential model. (b) Equivalent circuit of the passive circuitry.

Table 1: Component values used for the three control DUT data sets.

	$\mathbf{Z_{T_A}}$			$\mathbf{Z_{T_B}}$		
Data set	$R_1(\Omega)$	$R_2(\text{k}\Omega)$	$C_1(\text{nF})$	$R_4(\Omega)$	$R_3(\text{k}\Omega)$	$C_2(\text{nF})$
1	998.2	333.5	3.4	998.8	219.5	0.96
2	998.2	46.9	1,029.0	998.8	47.2	1,000
3	998.2	333.5	1.2	998.8	219.5	1.1

$$\text{NRMSE} = 100 \times \frac{\text{RMSE}}{\overline{Z}_T}\,, \tag{7}$$

where $\overline{Z}_T$ is the mean of the theoretical impedance,

$$\overline{Z}_T = \frac{1}{K}\sum_{k=0}^{K-1} Z_T(f_k)\,. \tag{8}$$

3.2.2 Human Subjects

To further validate human values for $Z_{A_{\text{CIA}}}(f)$ and $Z_{B_{\text{CIA}}}(f)$ obtained using the CIA, a Keysight Technologies E4990A impedance analyser (KIA) was used. The KIA has an excitation frequency range of 20 Hz–20 MHz, however, a 20 Hz–1 MHz range with 201 samples was implemented for this study. To compare the CIA and KIA data sets, interpolation and truncation of the data had to be performed. The KIA data was truncated to the first data point below or equal to 100 kHz (97.7 kHz) for the magnitude data and 10 kHz (9.5 kHz) for the phase data. The CIA data were up-sampled using cubic spline interpolation, then truncated. This process produced data sets that had a frequency span of 20 Hz–97.7 kHz for the magnitude data and 20 Hz–9.5 kHz for the

phase data. Both the magnitude and phase data sets were sampled at the same fixed frequencies for comparison.

Measuring the electrode-skin impedance at 50 Hz was avoided since coupled mains interference can effect the measurement. The interpolated data was used for $Z_{A_{\text{CIA}}}(f)$ and $Z_{B_{\text{CIA}}}(f)$ at 50 Hz. Besides the impedance at mains frequency, the interpolated data was only used in the validation process. The 100 kHz–1 MHz data from the KIA was not used in the validation process, but it gave valuable insight to the high frequency characteristics of the electrode-skin interface.

As the impedance measurements from the CIA are independent of the reference electrode impedance, a single excitation method using two electrodes was used to produce the KIA data. This ensures that a change in reference electrode impedance does not effect the impedance data, however, a two electrode configuration with a single excitation can only measure the combined impedance across the two electrode-skin interfaces, $Z_{\text{AB}_{\text{KIA}}}$. Therefore, the sum of the CIA data was used in the validation process. This is determined using,

$$|Z_{AB_{\text{CIA}}}(f)| = \sqrt{\left[\mathbb{R}\{Z_{A_{\text{CIA}}}(f)\} + \mathbb{R}\{Z_{B_{\text{CIA}}}(f)\}\right]^2 + \left[\mathbb{I}\{Z_{A_{\text{CIA}}}(f)\} + \mathbb{I}\{Z_{B_{\text{CIA}}}(f)\}\right]^2}, \tag{9}$$

$$\phi_{AB_{\text{CIA}}}(f) = \arctan\left[\frac{\mathbb{I}\{Z_{A_{\text{CIA}}}(f)\} + \mathbb{I}\{Z_{B_{\text{CIA}}}(f)\}}{\mathbb{R}\{Z_{A_{\text{CIA}}}(f)\} + \mathbb{R}\{Z_{B_{\text{CIA}}}(f)\}}\right], \tag{10}$$

where $\mathbb{R}(Z)$ symbolises the real component and $\mathbb{I}(Z)$ symbolises the imaginary component. A NRMSE was used to quantify the accuracy of the magnitude and phase of the CIA,

$$Z_{\text{NRMSE}} = 100 \times \frac{\frac{1}{K}\sqrt{\sum_{k=0}^{K-1}\left\{|Z_{\text{AB}_{\text{CIA}}}(f_k)| - |Z_{\text{AB}_{\text{KIA}}}(f_k)|\right\}^2}}{|\overline{Z}_{AB_{\text{KIA}}}|}, \tag{11}$$

$$\phi_{\text{NRMSE}} = 100 \times \frac{\frac{1}{K}\sqrt{\sum_{k=0}^{K-1}\left\{\phi_{\text{AB}_{\text{CIA}}}(f_k) - \phi_{\text{AB}_{\text{KIA}}}(f_k)\right\}^2}}{\overline{\phi}_{AB_{\text{KIA}}}}, \tag{12}$$

where $|\overline{Z}_{AB_{\text{KIA}}}|$ is the mean magnitude of $Z_{\text{AB}_{\text{KIA}}}$ and $\overline{\phi}_{AB_{\text{KIA}}}$ is the mean phase of $Z_{\text{AB}_{\text{KIA}}}$.

3.3 Electrode-skin Impedance Imbalance Metric

A RMSE between $\mathbf{Z}_{A_{\text{CIA}}}(f)$ and $\mathbf{Z}_{B_{\text{CIA}}}(f)$ was used to quantify the imbalance of the electrode-skin impedance. The metric was not normalised as bioelectrical signal interference is a function of the absolute impedance imbalance. The RMSE was calculated for the bioelectrical signal range (1 Hz–500 Hz [25]), the entire data range and mains frequency. Using the truncated data, this resulted in a bioelectrical signal range of 1 Hz–492.4 Hz, and an entire data range of 1 Hz–100 kHz magnitude and 1 Hz–9.4 kHz phase. The electrode-skin impedance imbalance at mains frequency (50 Hz) was calculated using the interpolated data.

3.4 Electrode Configurations

The electrode-skin impedance was measured for three different electrode configurations: silver/silver chloride disc electrodes without skin preparation ($Ag/AgCl_{NSP}$), silver/silver chloride disc electrodes with skin preparation ($Ag/AgCl_{SP}$), and silver bar electrodes with skin preparation (Ag_{SP}). Measuring the electrode-skin impedance using Ag electrodes without skin preparation was not performed, due to skin preparation being required to measure the sEMG signals using the Ag electrodes.

The Ag bar electrodes are imbedded within the CIA. When the excitation current from the KIA was applied to the Ag electrodes, the excitation current would also backfeed through the CIA. The multiple current paths resulted in erroneous impedance measurements, therefore, there is no validation data using the KIA for the Ag_{SP} electrode configuration. Backfeeding current using the Ag/AgCl electrodes was avoided as the electrode leads could be disconnected from the CIA without disrupting the electrode-skin interface.

3.5 Subject Data

This study was approved by the Human Ethics Committee, University of Canterbury (HEC 2019/68). Data from ten healthy subjects (five male and five female with a mean age of 25 ± 4) were collected for this study. The first data set collected was for the $Ag/AgCl_{NSP}$ electrodes, where the electrodes were placed above the right biceps brachii muscle belly. The second recorded data set was for the Ag_{SP} electrodes, placed above the left biceps brachii muscle belly and the last data set was for the $Ag/AgCl_{SP}$ electrodes, also placed above the left biceps brachii muscle belly. This order of recording ensured the adhesive and electrode gel from the Ag/AgCl electrodes did not affect the impedance of the succeeding recordings. Another Ag/AgCl electrode was placed on the elbow to use as the reference electrode. This electrode configuration mimics the set up typically used during sEMG for recording the electrical activity of the biceps brachii.

The Ag/AgCl electrodes were VERMED VersaTrode, polyethylene foam, single use, wet gel teardrop electrodes. The adhesive foam had a diameter of 38.1 mm, and the electrode eyelet was 10.6 mm in diameter, resulting in an interelectrode distance of approximately 40 mm. The CIA had imbedded Ag electrodes, constructed from 1 mm round, 99.99% pure, silver wire, producing a 1x10 mm electrode, with a 10 mm interelectrode distance. The skin preparation was achieved using 600 grit sand paper. The skin surface was abraded using approximately 20 light uniform sweeps over a large area above the biceps brachii to reduce the possibility of producing a local area of impedance difference related to variations in skin preparation. The skin surface was sterilised using alcohol pads, 75% Ethyl Alcohol, and left for a minimum of two minutes to dry. The subjects were required to relax their arm on a table, while maintaining an elbow angle of approximately 90 degrees. The KIA is sensitive to electrostatic discharge (ESD), therefore, to protect the device and maintain consistency, an ESD band was worn for all recordings. The impedance measurements were not effected by the ESD band.

3.6 Electrode-skin Impedance Compensation

A data-driven electrode-skin impedance compensation network was developed to reduce the impedance imbalance of the electrode-skin interface, therefore, reducing the common-mode to differential-mode conversion caused by the potential divider effect. As the electrode-skin

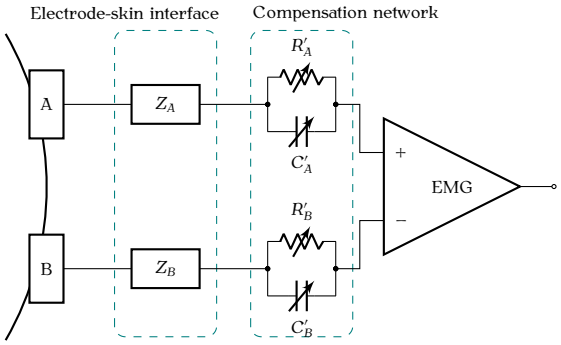

Figure 3: High level schematic of the electrode-skin interface (using a generic impedance) and compensation network.

impedance is non-linear, a non-linear electrode-skin impedance compensation network is required. The compensation network is designed to go in series with the electrodes, Figure 3, where R'_A and C'_A are the variable compensation components for electrode A, and R'_B and C'_B are the variable compensation components for electrode B. These components will be digitally tunable, allowing the electrode-skin impedance to be measured and automatically balanced. As the electrode-skin impedance has a temporal relationship, the electrode-skin impedance will need to be measured and balanced repeatedly.

Non-linear least squares (NLLS) regression was used to simultaneously minimise the magnitude and phase imbalance of the experimental electrode-skin impedance data, therefore, simulating electrode-skin impedance compensation. As the residual error was a function of both magnitude and phase, the frequency range was limited to that of the phase data (1 Hz–9.4 kHz). The NLLS regression was implemented using the interior point algorithm in MATLAB (R2019b, MathWorks). The bounds of the NLLS regression was set to physical limits desired for the compensation network. The resistive components were bound between 1 Ω and 10 MΩ, and the capacitive elements were bound between 1 nF and 10 μF. To reduce the possibility of a solution being based on a local minima, the NLLS regression was run 100 times. The first 50 initial value vectors were formed using the lower and upper bounds in a logarithmically ascending order. The same method was used to produce the remaining 50 initial value sets; however, R'_B and C'_B had a logarithmically descending order. Initially the NLLS regression was run using coarse exit conditions to decrease the processing time of the solver. The initial conditions that resulted in the least error, were run again with finer exit criteria. A RMSE between the two compensated impedance data sets was calculated over the phase data frequency span, permitting a quantitative simulated impedance imbalance reduction.

4 Results

4.1 Proxy Device Under Test (DUT)

The accuracy of the CIA using the proxy DUT is outlined in Table 2, resulting in a mean error and standard deviation of (4.6 ± 0.7) % for the magnitude and (2.6 ± 0.9) % for the phase of electrode A; and (5.3 ± 0.6) % for the magnitude and (3.6 ± 2.0) % for the phase of electrode B. These results indicate that impedance measurement methods using the CIA can accurately

Table 2: Error between the custom impedance analyser (CIA) and the theoretical impedance of the control DUT over the range of 1 Hz–100 kHz (magnitude) and 1 Hz–10 kHz (phase), quantified by the root-mean-square error normalised using the mean of the theoretical impedance of the control DUT.

	$\mathbf{Z_A}$		$\mathbf{Z_B}$	
Data set	$\lvert Z\rvert$ (%)	ϕ (%)	$\lvert Z\rvert$ (%)	ϕ (%)
1	4.7	2.7	5.7	5.3
2	5.3	1.6	5.6	1.5
3	3.8	3.4	4.6	4.2
Mean (SD)	4.6 (0.7)	2.6 (0.9)	5.3 (0.6)	3.6 (2.0)

Table 3: Error between the custom impedance analyser (CIA) and the Keysight impedance analyser (KIA) measured combined impedance of electrodes A and B on human subjects over the range of 1 Hz–100 kHz (magnitude) and 1 Hz–9.4 kHz (phase), quantified by the root-mean-square error normalised using the mean of the KIA.

	$\mathbf{Ag/AgCl_{NSP}}$		$\mathbf{Ag/AgCl_{SP}}$	
Subject	$\lvert Z\rvert$ (%)	ϕ (%)	$\lvert Z\rvert$ (%)	ϕ (%)
1	3.3	0.9	1.7	14.9
2	7.6	3.7	6.4	11.3
3	14.4	2.7	3.4	4.4
4	1.8	0.8	1.2	24.0
5	16.9	1.7	1.6	19.0
6	9.4	0.6	3.2	4.2
7	4.4	1.3	17.4	5.5
8	64.8	12.8	11.3	9.8
9	1.5	0.9	8.6	4.2
10	0.8	1.1	2.6	8.9
Mean (SD)	12.5 (19.2)	2.7 (3.7)	5.7 (5.3)	10.6 (6.8)

measure magnitude up to 100 kHz, and phase up to 10 kHz.

4.2 Subject Trial

The accuracy of the CIA for the ten subjects is outlined in Table 3, resulting in a mean error and standard deviation of (12.5 ± 19.2) % for the magnitude and (2.7 ± 3.7) % for the phase using the $Ag/AgCl_{NSP}$ electrode configuration, and (5.7 ± 5.3) % for the magnitude and (10.6 ± 6.8) % for the phase using the $Ag/AgCl_{SP}$ electrode configuration.

The imbalance of the electrode-skin interface for the ten subjects and three electrode configurations as measured by the CIA is outlined in Table 4, resulting in a mean imbalance and standard deviation at mains frequency (50 Hz) of (37.6 ± 47.1) kΩ for the magnitude and (15.0 ± 18.3) degrees for the phase using the $Ag/AgCl_{NSP}$ electrode configuration, (4.52 ± 7.65) kΩ for the magnitude and (4.6 ± 6.9) degrees for the phase using the $Ag/AgCl_{SP}$ electrode configuration, and (36.2 ± 45.1) kΩ for the magnitude and (3.4 ± 3.6) degrees for the phase using the $Ag_{\text{-SP}}$ electrode configuration. As the standard deviation is larger than the mean, and the data is non negative, the data has a right skewed distribution.

Data from subjects 4, 7 and 10 for the three electrode configurations are presented in Figures 4, 5 and 6. These subjects were chosen because they show a range of interesting results. Subject 4 had the least balanced magnitude data over the bioelectrical signal range ($Ag/AgCl_{NSP}$ electrode configuration), and the most balanced data set ($Ag/AgCl_{SP}$ electrode configuration); Subject 7 had the largest recording error ($Ag/AgCl_{NSP}$ electrode configuration, but as the recording error is below 20 Hz, the validation error is still low), and the least balanced data set at 50 Hz (Ag_{SP} electrode configuration); Subject 10 had the least balanced phase data set ($Ag/AgCl_{NSP}$ electrode configuration).

4.3 Electrode-skin Impedance Compensation

The mean and standard deviation of the electrode-skin impedance imbalance and the reduction in impedance imbalance after applying the compensation network are outlined in Table 5. The mean and standard deviation of the compensation network component values are outlined in Table 6. Compensation data for Subjects 4, 7 and 10 for the $Ag/AgCl_{NSP}$ electrode configuration are shown in Figure 7. This electrode configuration was chosen as it was the most imbalanced. These results highlight the potential for a compensation network to reduce the impedance imbalance of the electrode-skin interface, therefore, reducing differential-mode interference due to the potential divider effect.

5 Discussion

The validation error between the CIA and the KIA is typically low. However, 25% of the validated recordings have a NRMSE above 10%, where most of these data sets had a small absolute phase leading to a large relative error. It is believed the temporal relationship of the electrode-skin impedance is the main cause for the NRMSE. The impedance measuring process had a set-up time after electrode placement of 2–5 minutes, with recording times of 9.7 ± 2.3 minutes. Due to the large validation error of Subject 8, a 15 minute wait period was performed between applying the $Ag/AgCl_{NSP}$ electrodes and recording the impedance for Subjects 9 and 10, resulting in the lowest validation errors of the study. As the electrode-skin impedance and frequency have an inverse relationship, and the interface is more susceptible to time variance at low frequencies, the time dependence of the interface has a large impact on the validation error. Due to this phenomenon, it is believed the CIA can accurately measure the impedance of the electrode-skin interface.

Skin preparation is a good method to reduce electrode-skin impedance imbalance: Subject 4 went from the largest recorded magnitude imbalance (1.4 MΩ for the bioelectrical signal range using the $Ag/AgCl_{NSP}$ electrode configuration) to the lowest recorded magnitude imbalance (50 Ω for the bioelectrical signal range using the $Ag/AgCl_{SP}$ electrode configuration). However, this level of abrasion is not suitable for subjects with sensitive skin, existing skin irritations, those requiring frequent recordings, or infants. Although skin preparation lowers the electrode-skin impedance, it does not guarantee a balanced electrode-skin interface. This is highlighted when comparing the impedance imbalance at 50 Hz and over the bioelectrical signal range.

Multiple methods were applied to reduce limitations of this study. During skin preparation, approximately 20 light uniform sweeps over a large area above the biceps brachii were performed. This reduced the possibility of skin preparation producing an impedance imbalance. To ensure the electrode adhesive and gel did not effect the impedance measurements between

Table 4: Electrode-skin impedance imbalance quantified using a root mean square error between Z_A and Z_B for ten healthy subjects over three different frequency ranges: 50 Hz, 1 Hz–492.4 Hz and the entire range, 1 Hz–100 kHz (magnitude) and 1 Hz–9.4 kHz (phase).

$Ag/AgCl_{NSP}$

	50 Hz		**Bio-signal range**		**Whole range**	
Subject	$\|Z\|\,(k\,\Omega)$	$\phi\,(deg)$	$\|Z\|\,(k\,\Omega)$	$\phi\,(deg)$	$\|Z\|\,(k\,\Omega)$	$\phi\,(deg)$
1	20.6	16.2	473.0	30.1	350.8	25.1
2	9.2	4.7	9.8	3.8	7.3	3.4
3	12.5	6.7	13.8	4.7	10.3	4.0
4	2.8	12.4	1,447.0	14.8	1,073.1	12.3
5	120.5	14.8	142.8	16.2	106.0	13.6
6	116.9	10.1	264.3	12.4	196.1	10.4
7	21.6	10.0	298.9	7.8	221.7	6.6
8	2.1	6.4	32.6	6.6	24.2	5.6
9	0.9	2.7	82.4	4.1	61.1	3.4
10	69.2	65.5	607.1	56.3	450.3	47.7
Mean (SD)	37.6 (47.1)	15.0 (18.3)	337.2 (439.3)	15.7 (16.4)	250.1 (325.8)	13.2 (13.8)

$Ag/AgCl_{SP}$

	50 Hz		**Bio-signal range**		**Whole range**	
Subject	$\|Z\|\,(k\,\Omega)$	$\phi\,(deg)$	$\|Z\|\,(k\,\Omega)$	$\phi\,(deg)$	$\|Z\|\,(k\,\Omega)$	$\phi\,(deg)$
1	0.3	0.0	0.3	1.1	0.2	3.2
2	1.4	1.1	1.4	3.8	1.1	10.9
3	8.3	6.6	8.3	11.5	6.3	23.2
4	0.1	0.7	0.1	0.6	0.0	1.5
5	0.2	0.0	0.2	0.7	0.2	1.6
6	1.8	2.0	1.9	3.3	1.4	6.5
7	24.6	22.2	29.4	21.6	21.8	21.9
8	1.3	4.0	1.3	6.7	1.0	14.1
9	7.0	9.2	6.9	15.1	5.1	22.2
10	0.3	0.5	0.3	1.2	0.3	4.8
Mean (SD)	4.5 (7.7)	4.6 (6.9)	5.0 (9.0)	6.6 (7.2)	3.8 (6.7)	11.0 (8.8)

$Ag_{\text{-SP}}$

	50 Hz		**Bio-signal range**		**Whole range**	
Subject	$\|Z\|\,(k\,\Omega)$	$\phi\,(deg)$	$\|Z\|\,(k\,\Omega)$	$\phi\,(deg)$	$\|Z\|\,(k\,\Omega)$	$\phi\,(deg)$
1	7.8	1.5	12.5	2.0	9.3	4.5
2	37.4	1.5	39.4	6.5	29.4	7.4
3	63.8	1.3	113.1	7.2	83.9	7.6
4	7.4	2.8	16.1	2.8	12.0	2.6
5	0.8	0.4	0.8	0.8	0.6	1.8
6	14.9	1.0	39.0	2.6	28.9	3.8
7	143.2	10.4	245.2	10.4	181.9	9.3
8	0.8	3.0	13.6	4.9	10.1	4.1
9	69.3	9.8	529.6	6.2	39.3	5.2
10	16.6	2.2	26.4	3.2	19.6	4.4
Mean (SD)	36.2 (45.1)	3.4 (3.6)	103.6 (166.8)	4.7 (2.9)	76.9 (123.7)	5.1 (2.3)

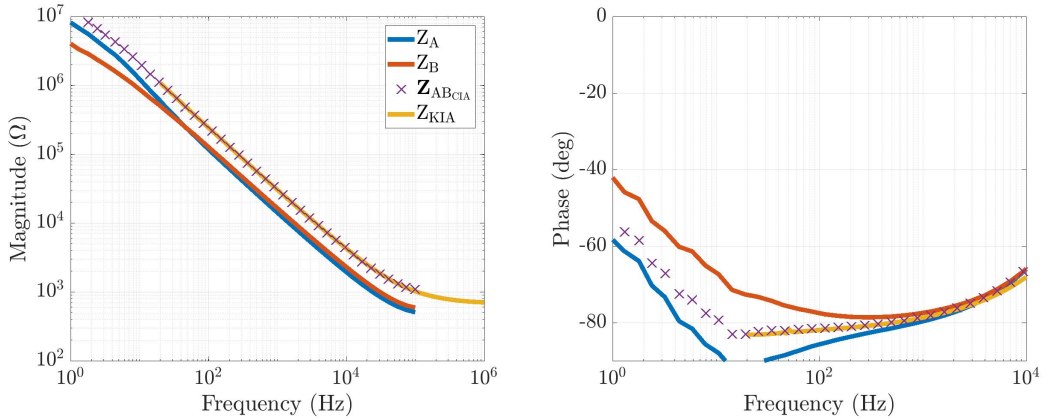

(a) Subject 4: least balanced (magnitude) data set (1 Hz–500 Hz).

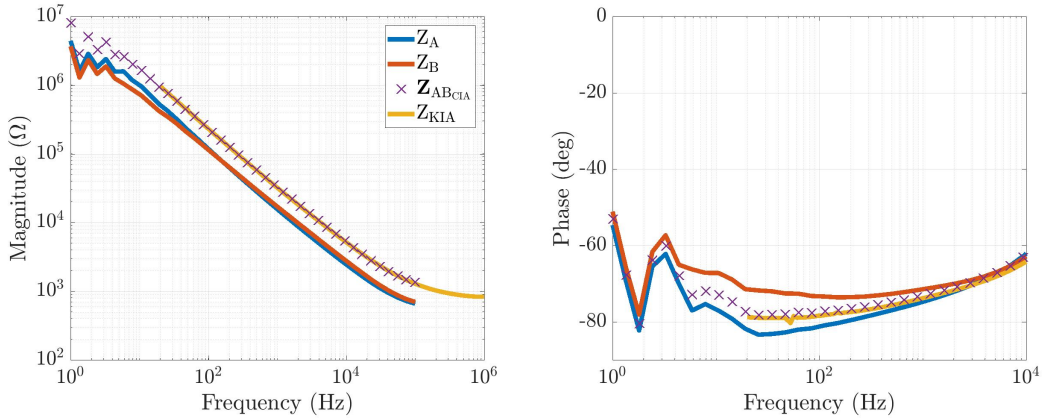

(b) Subject 7: largest recording error data set.

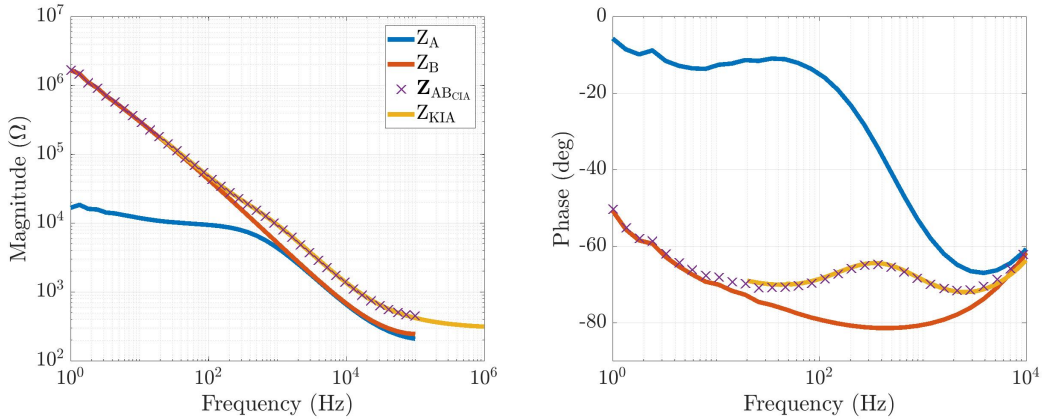

(c) Subject 10: least balanced (phase) data set.

Figure 4: Electrode-skin impedance imbalance for 3 healthy subjects using $Ag/AgCl_{NSP}$ electrodes.

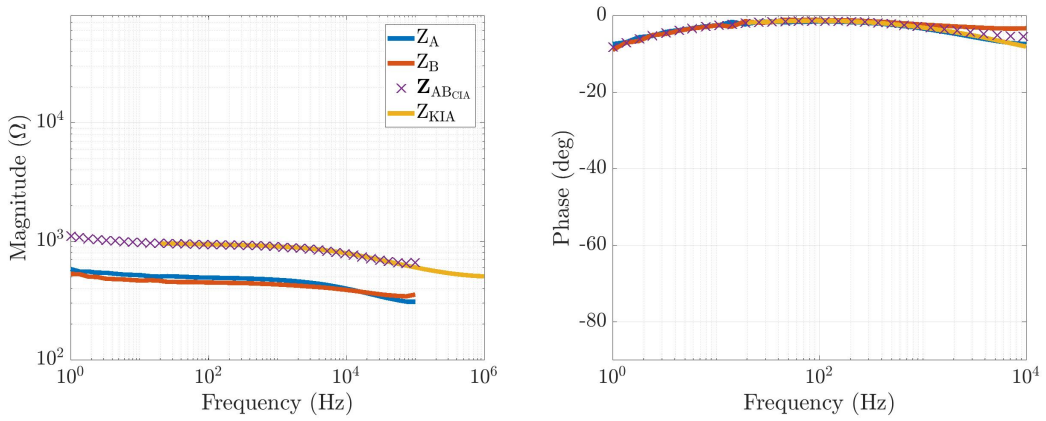

(a) Subject 4: most balanced data set.

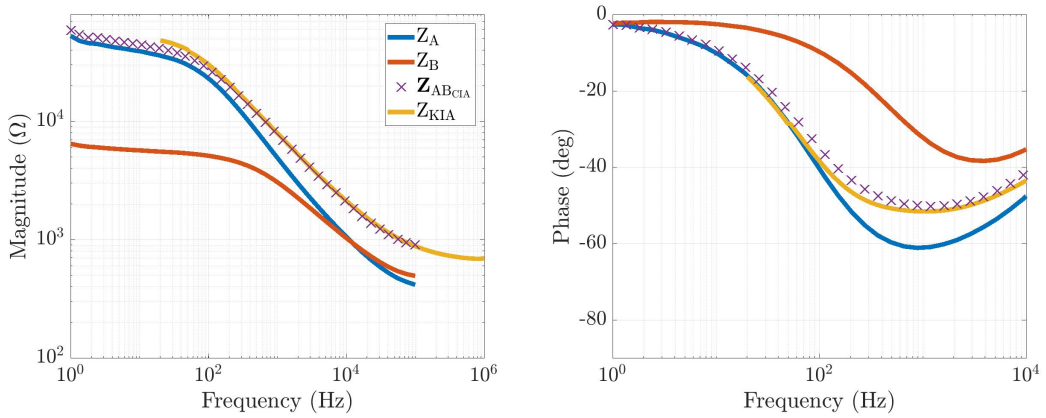

(b) Subject 7.

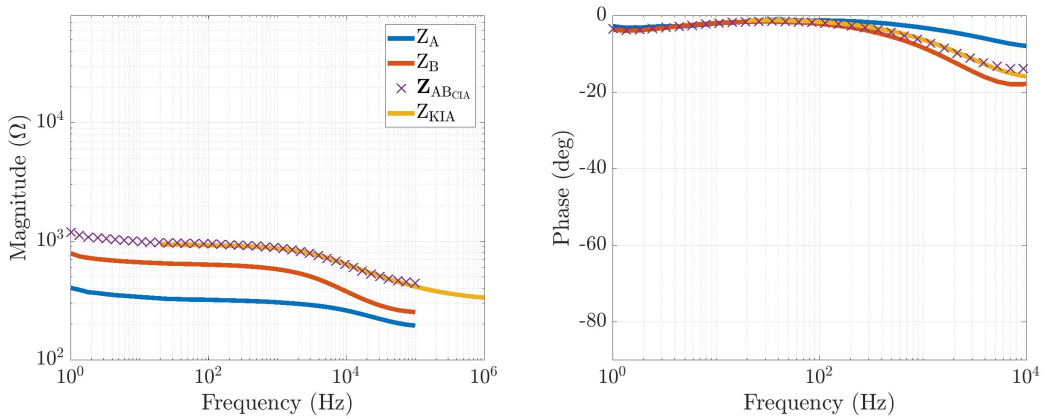

(c) Subject 10.

Figure 5: Electrode-skin impedance imbalance for 3 healthy subjects using $Ag/AgCl_{SP}$ electrodes. Note the impedance is substantially lower due to the skin preparation.

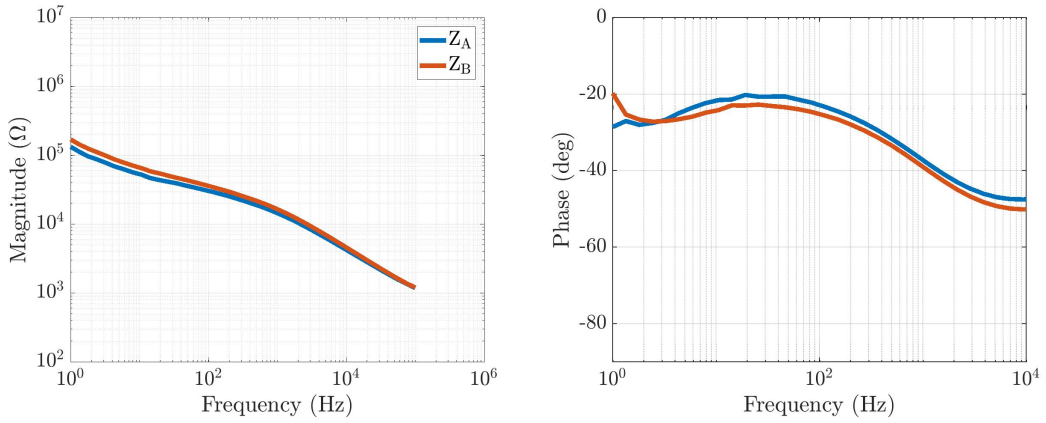

(a) Subject 4.

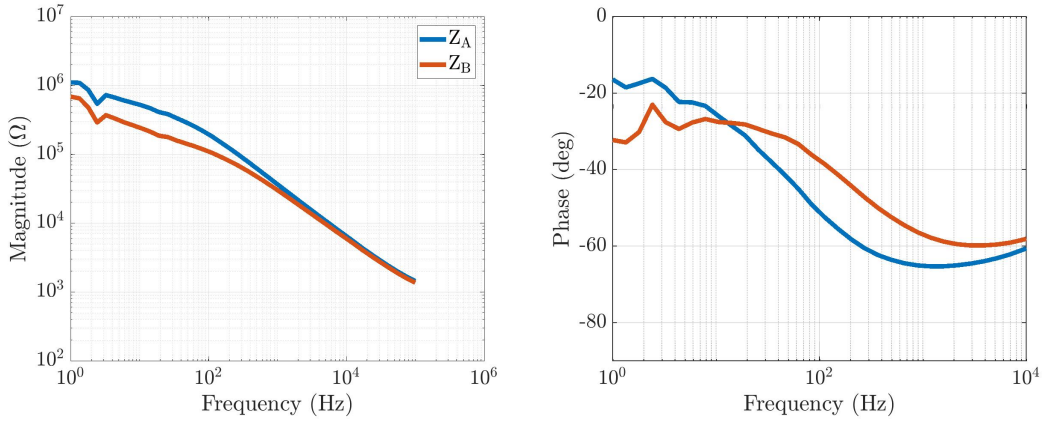

(b) Subject 7: least balanced at 50 Hz (143.2 kΩ).

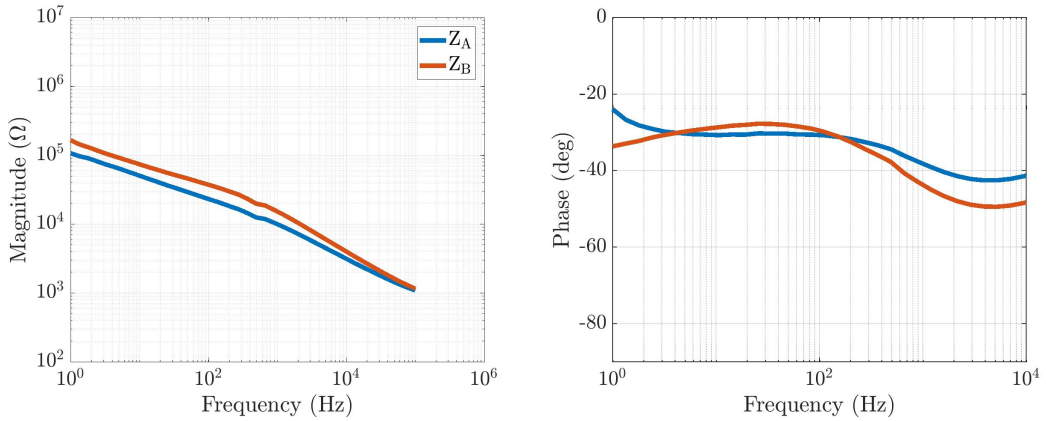

(c) Subject 10.

Figure 6: Electrode-skin impedance imbalance for 3 healthy subjects using Ag_{-SP} electrodes.

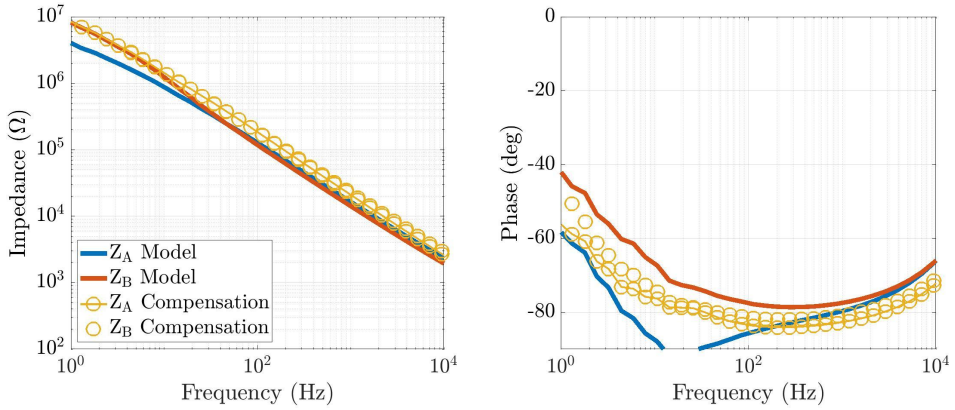

(a) Subject 4: least balanced (magnitude) data set (1 Hz–500 Hz).

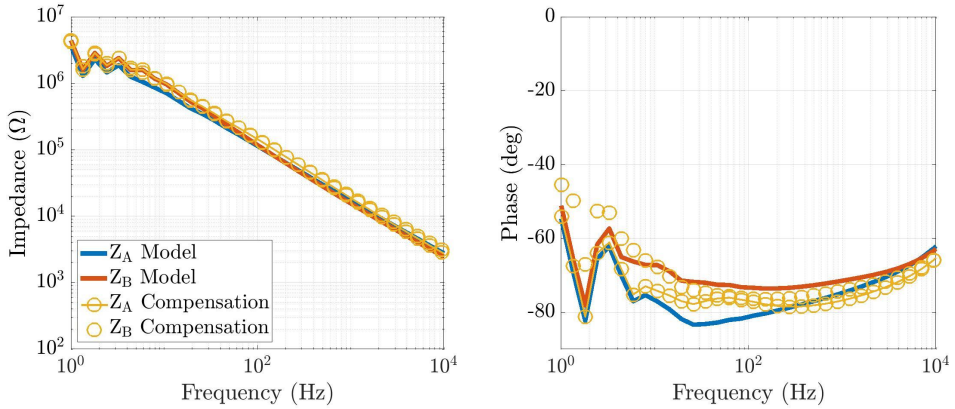

(b) Subject 7: largest recording error data set.

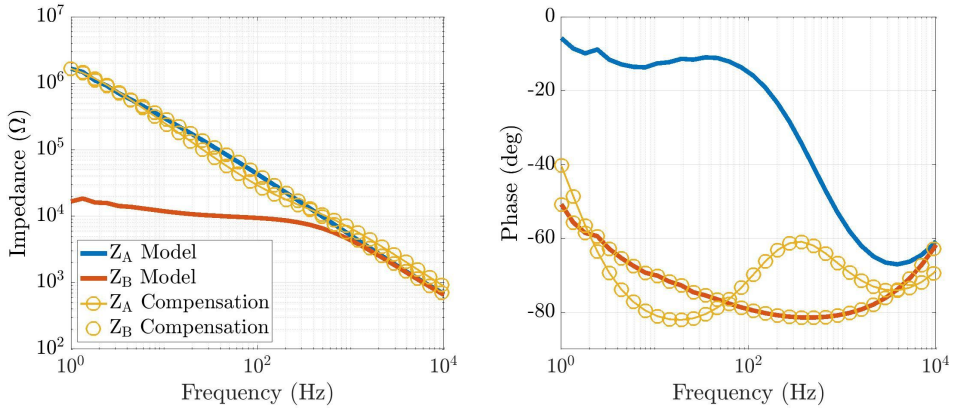

(c) Subject 10: least balanced (phase) data set.

Figure 7: Electrode-skin impedance compensation for 3 healthy subjects using $Ag/AgCl_{NSP}$ electrodes.

Table 5: Mean electrode-skin impedance imbalance and imbalance reduction after applying the compensation network, quantified using a root mean square error between Z_A and Z_B over 1 Hz–9.4 kHz.

	Absolute Imbalance		Imbalance Reduction	
Electrode configuration	$\|Z\|$ (kΩ)	ϕ (deg)	$\|Z\|$ (kΩ)	ϕ (deg)
$Ag/AgCl_{NSP}$	25.0 ± 29.0	3.8 ± 2.1	284.3 ± 361.8	11.9 ± 15.8
$Ag/AgCl_{SP}$	0.4 ± 1.0	0.3 ± 0.6	4.6 ± 8.1	6.2 ± 6.7
Ag_{-SP}	12.9 ± 15.4	2.2 ± 1.4	86.7 ± 143.1	2.5 ± 2.3

Table 6: Mean and standard deviation of the compensation network component values.

Electrode configuration	R'_A (kΩ)	C'_A (nF)	R'_B (kΩ)	C'_B (nF)
$Ag/AgCl_{NSP}$	1,884 ± 3,158	144.8 ± 237.2	1,748 ± 1,886	141.8 ± 207.4
$Ag/AgCl_{SP}$	99.6 ± 115.2	6.6 ± 9.9	102.9 ± 118.6	6.8 ± 10.4
Ag_{-SP}	2,811 ± 3,736	202.2 ± 403.7	2,816 ± 3,465	487.9 ± 1,153

the different electrode configurations, the $Ag/AgCl_{NSP}$ electrode-skin impedance was measured on the right arm, and the $Ag/AgCl_{SP}$ electrode-skin impedance was measured on the left arm. This does have the limitation that the impedance imbalance will vary from limb-to-limb. However, the issue that an impedance imbalance can be present after skin preparation is proven. The impedance imbalance of the Ag_{-SP} and $Ag/AgCl_{SP}$ electrode-skin interfaces were measured on the same arm, but due to electrode size, the interelectrode distance was different. However, the large area of uniformly prepared skin should have resulted in an interface with similar characteristics.

An electrode-skin interface using $Ag/AgCl_{SP}$ electrodes is the most likely interface to achieve the lowest imbalance. However, there are other performance parameters to consider between Ag and Ag/AgCl electrodes: interelectrode distance, adhesive properties, half-cell potentials and single-use verse multiple-use electrodes. Regardless of preferred electrode type and skin preparation method, Ag and Ag/AgCl electrodes will inherently produce an imbalanced electrode-skin interface.

The compensation network was successful in reducing the electrode-skin impedance imbalance. However, in a physical system the compensation component values are limited to discrete values, therefore, limiting the efficacy of the compensation network. Modelling the electrode-skin interface has the potential to provide quantitative insight that may assist in calculating initial estimates for the NLLS regression, further limiting the occurrence of local minima solutions, therefore, further reducing the electrode-skin impedance imbalance and the associated bioelectrical-signal interference.

Electrode-skin impedance imbalance exists, where the extent varies across different subjects, skin preparation levels, electrode material and time. However, the proposed compensation network has the potential to reduce the electrode-skin impedance imbalance. As the electrode-skin impedance imbalance causes interference within bioelectrical recordings, the imbalance of the electrode-skin impedance cannot be ignored.

6 Conclusion

Although abrasive skin preparation reduces the electrode-skin impedance imbalance, it does not guarantee a balanced electrode-skin interface. As there is no commercial product to determine the impedance imbalance of the interface, it is difficult to verify that the electrode-skin interface is balanced, particularly if the imbalance at mains frequency is low compared to the bioelectrical signal range.

Typically when the impedance imbalance of the electrode-skin interface is investigated, only the magnitude of the imbalance is considered. However, the phase can also be imbalanced. The results from this study indicate that the electrode-skin impedance imbalance ranges from 0.1–143.2 kΩ and 0.0–22.2 degrees, where the largest magnitude imbalance is not associated with the largest phase imbalance. The electrode-skin impedance imbalance is time variant, and is inconsistent between subjects, electrode type and skin preparation. A compensation network was proposed and simulated on the electrode-skin impedance data, resulting in a mean reduction in impedance imbalance over the bioelectrical signal range of 284.3 kΩ and 11.9 degrees; 4.6 kΩ and 6.2 degrees; 86.7 kΩ and 2.5 degrees for the $Ag/AgCl_{NSP}$, $Ag/AgCl_{SP}$ and Ag_{SP} electrode configurations respectively. Therefore, to improve the noise immunity of bioelectrical signal recordings, repeated monitoring and automatic compensation is required to balance the electrode-skin interface.

References

[1] B. B. Winter and J. G. Webster, "Reduction of Interference Due to Common Mode Voltage in Biopotential Amplifiers," *IEEE Transactions on Biomedical Engineering*, vol. BME-30, pp. 58–62, Jan. 1983.

[2] J. C. Huhta and J. G. Webster, "60-Hz Interference in Electrocardiography," *IEEE Transactions on Biomedical Engineering*, vol. BME-20, pp. 91–101, Mar. 1973.

[3] Van Rijn Metting, AC, Peper, A, and Grimbergen, CA, "High-quality recording of bioelectric events," *Springer*, vol. 28, no. 5, pp. 389–397, 1990.

[4] A. F. Pacela, "Collecting the body's signals," *Electronics*, vol. 40, pp. 103–112, 1967.

[5] J. Webster, *Medical instrumentation: application and design*. John Wiley & Sons, 2009.

[6] J. M. Kilner, S. N. Baker, and R. N. Lemon, "A novel algorithm to remove electrical cross-talk between surface EMG recordings and its application to the measurement of short-term synchronisation in humans," *The Journal of Physiology*, vol. 538, pp. 919–930, Feb. 2002.

[7] D. Farina, R. Merletti, B. Indino, M. Nazzaro, and M. Pozzo, "Surface EMG crosstalk between knee extensor muscles: Experimental and model results," *Muscle & Nerve*, vol. 26, pp. 681–695, Nov. 2002.

[8] C. J. De Luca, M. Kuznetsov, L. D. Gilmore, and S. H. Roy, "Inter-electrode spacing of surface EMG sensors: Reduction of crosstalk contamination during voluntary contractions," *Journal of Biomechanics*, vol. 45, pp. 555–561, Feb. 2012.

[9] V. S. Selvanayagam, S. Riek, and T. J. Carroll, "A systematic method to quantify the presence of cross-talk in stimulus-evoked EMG responses: Implications for TMS studies," *Journal of Applied Physiology*, vol. 112, pp. 259–265, Jan. 2012.

[10] Loeb, Gerald E and Gans, Carl, *Electromyography for experimentalists*. University of Chicago Press, 1986.

[11] J. P. P. Van Vugt and J. G. Van Dijk, "A convenient method to reduce crosstalk in surface EMG," *Clinical Neurophysiology*, vol. 112, no. 4, pp. 583–592, 2001.

[12] C. J. De Luca and R. Merletti, "Surface myoelectric signal cross-talk among muscles of the leg," *Electroencephalography and Clinical Neurophysiology*, vol. 69, pp. 568–575, June 1988.

[13] T. J. Koh and M. D. Grabiner, "Evaluation of methods to minimize cross talk in surface electromyography," *Journal of biomechanics*, vol. 26, pp. 151–157, 1993.

[14] Y.-K. Kong, M. S. Hallbeck, and M.-C. Jung, "Crosstalk effect on surface electromyogram of the forearm flexors during a static grip task," *Journal of Electromyography and Kinesiology*, vol. 20, pp. 1223–1229, Dec. 2010.

[15] J. J. Almasi and O. H. Schmitt, "Systemic and Random Variations of Ecg Electrode System Impedance," *Annals of the New York Academy of Sciences*, vol. 170, no. 2, pp. 509–519, 1970.

[16] E. T. McAdams, *A study of electrode-tissue impedances encountered in cardiac pacing*. PhD thesis, University of Leeds, 1987.

[17] W. H. Olson, D. R. Schmincke, and B. L. Henley, "Time and frequency dependence of disposable ECG electrode-skin impedance.," *Medical instrumentation*, vol. 13, no. 5, pp. 269–272, 1979.

[18] S. Grimnes, "Impedance measurement of individual skin surface electrodes," *Medical and Biological Engineering and Computing*, vol. 21, no. 6, pp. 750–755, 1983.

[19] S. Nag, S. K. Sikdar, N. V. Thakor, V. R. Rao, and D. Sharma, "Sensing of Stimulus Artifact Suppressed Signals From Electrode Interfaces," *IEEE Sensors Journal*, vol. 15, pp. 3734–3742, July 2015.

[20] J. R. Cram and D. Rommen, "Effects of skin preparation on data collected using an EMG muscle-scanning procedure," *Applied Psychophysiology and Biofeedback*, vol. 14, no. 1, pp. 75–82, 1989.

[21] C. Assambo, A. Baba, R. Dozio, and M. J. Burke, "Determination of the parameters of the skin-electrode impedance model for ECG measurement," in *Proceedings of the 6th WSEAS international conference on electronics, hardware, wireless and optical communications, Corfu Island, Greece*, pp. 90–95, 2007.

[22] L. Casal and G. L. Mura, "Skin-electrode impedance measurement during ECG acquisition: method's validation," *Journal of Physics: Conference Series*, vol. 705, p. 012006, Apr. 2016.

[23] H. Saadi and M. Attari, "Electrode-gel-skin interface characterization and modeling for surface biopotential recording: Impedance measurements and noise," in *2013 2nd International Conference on Advances in Biomedical Engineering*, pp. 49–52, Sept. 2013.

[24] I. Zepeda-Carapia, A. Marquez-Espinoza, and C. Alvarado-Serrano, "Measurement of skin-electrode impedance for a 12-lead electrocardiogram," in *2005 2nd International Conference on Electrical and Electronics Engineering*, pp. 193–195, Sept. 2005.

[25] Carlo J. De Luca, "The Use of Surface Electromyography in Biomechanics," *Journal of Applied Biomechanics*, vol. 13, pp. 135–163, May 1997.